Modeling heat and mass transfer across interfaces in two-phase flows using phase-field methods

By S. Mirjalili, S. S. Jain AND A. Mani

1. Motivation and objectives

Two-phase flow problems involving interfacial transfer of heat and mass are ubiquitous. Accurate prediction of interfacial heat transfer is critical in many industrial settings, including direct-contact heat exchangers (Nomura *et al.* 2013), distillation processes (Kister *et al.* 1992), combustion (Williams 1985), atomization of sprays (Lefebvre & McDonell 2017) and all problems that involve evaporation and boiling. Industrial applications where interfacial mass transfer plays an important role include bubble column reactors (Kantarci *et al.* 2005), oxygenation of aqueous systems (Orlebeke & Orlebeke 2009), metal refining, gas scrubbing and waste water treatments in bioreactors (Stephenson *et al.* 2000). Interfacial mass and heat transfer is also of significant interest in many natural phenomena, including rain formation and atmosphere-ocean heat/mass exchange [e.g., oceanic carbon sequestration (Lal 2008)].

To predict the evolution of heat and mass in the above applications numerically, it is critical to accurately compute (1) the evolution of the interface between two phases, (2) the transport—i.e., diffusion and advection—of heat/mass within the bulk of each phase, and (3) their transfer across the interface. There are plenty of effective and accurate numerical methods for capturing the interfaces in two-phase flows (Mirjalili *et al.* 2017). While sharp interface methods such as level-set (LS) and volume-of-fluid (VOF) methods have traditionally received the most attention, diffuse interface methods, also known as phase field methods, have recently become popular for simulating two-phase flows. This rise in popularity is due to their simplicity in implementation, parallel scalability and the possibility of using more standard finite-difference discretization schemes because of the diffuse interfaces that result in smooth fields. There has been a fair amount of previous work on the development of simulation techniques for transport and interfacial transfer of heat/mass in two-phase systems. These developments have been mostly for sharp interface methods. As we will show, there is an equivalence between the problems of heat transfer and mass transfer, and a numerical model designed for one can be reformulated for the other.

Broadly, the proposed models in the literature for either heat transfer problems or mass transfer problems can be classified into one-scalar models and two-scalar models. The former is based on the assumption of thermal equilibrium for heat and chemical equilibrium for mass at the interface—continuity of temperature for heat and Henry's law for mass. Examples of one-scalar models can be found in Bothe *et al.* (2004), Mehdi-Nejad *et al.* (2004), Deising *et al.* (2018) for VOF methods; Yang & Mao (2005), Wang *et al.* (2008) and Balcázar-Arciniega *et al.* (2019) for LS methods; and Zheng *et al.* (2015) for phase field methods. In these methods, a single equation is solved to compute the evolution of heat/mass within the two phases. The main drawback of one-scalar models is leakage in situations where the resistance (diffusivity) ratio between the two phases is large. Such situations are common in many practical gas-liquid two-phase flows. This has

motivated researchers to develop two-scalar models that can prevent leakage and yield more accurate transient solutions, as they do not enforce thermodynamic equilibrium at the interface but rather ensure that the steady solution to the model achieves thermodynamic equilibrium. Such models solve one equation for the heat/mass stored within each phase, resulting in two-scalar equations for two-phase flows. Notable examples of such models can be found in Davidson & Rudman (2002), Alke *et al.* (2009), Marschall *et al.* (2012), Bothe & Fleckenstein (2013) and Fleckenstein & Bothe (2015); all of these models are designed for VOF interface capturing schemes and most of them can also be adapted to other sharp interface schemes, i.e., LS methods.

The heat/mass diffusivity ratio is very large in many two-phase systems. As a result, in such systems the heat/mass is effectively confined to one of the phases. Some researchers have therefore developed transport models that do not account for interfacial transfer (Berry *et al.* 2013; Jain & Mani 2020). In particular, Jain & Mani (2020) derived one such model for phase field methods that prevents leakage across the interfaces, preserves the positivity of the scalar (heat/mass) and achieves an equilibrium profile for the scalar that is consistent with the phase field solution profiles. In this work, we extend the work of Jain & Mani (2020) by analytically deriving the interfacial transfer terms to obtain models that account for conjugate transfer of heat/mass. In particular, by assuming a microstructure for the interface, we use perturbation analysis to obtain transfer terms for the two-scalar model that are consistent with the phase field model. The derived two-scalar model can be applied to problems with arbitrary diffusivity ratios between the two phases. Additionally, by assuming thermodynamic equilibrium at the interface, we also derive a consistent one-scalar model that performs well when the two phases have comparable diffusivity for heat/mass but suffers from leakage when the diffusivity ratio is large.

In Section 2, we first explain that the problems of heat and mass transport in two-phase flows are equivalent, even discretely. Then, using a microscopic model for the diffuse interface, we derive the models for interfacial transfer of heat/mass. After describing the computational approach taken, we present several numerical tests of the models for validation in Section 3. Finally, we summarize our findings in Section 4.

2. Model for interfacial heat and mass transfer

2.1. *Governing equations*

Capillary interfaces are sharp in continuum scale. The governing equations for the evolution of heat/mass in a two-phase system thus consist of transport equations that hold within the bulk of each phase, in addition to boundary conditions at the interface, connecting the bulks lying on either side. The transport equation for the bulk fluids is an advection-diffusion equation. For mass transport, within the bulk of phase i we have

$$\frac{\partial \tilde{c}_i}{\partial t} + \nabla \cdot (\vec{u}\tilde{c}_i) = \nabla \cdot (D_i \nabla \tilde{c}_i), \tag{2.1}$$

where $i = 1, 2$, the diffusivity is denoted D and $\tilde{c}_i$ is the local species concentration in phase i defined as amount of the species per unit volume of phase i. At the interface, mass balance implies continuity of the fluxes normal to the interface,

$$D_1 \nabla_n \tilde{c}_1 = D_2 \nabla_n \tilde{c}_2. \tag{2.2}$$

The second-order partial differential equation (PDE) given in Eq. (2.1) requires one more boundary condition, which comes from chemical equilibrium at the interface, modeled by Henry's law,

$$\frac{\tilde{c}_1}{\tilde{c}_2} = H, \tag{2.3}$$

where H is the Henry coefficient, assumed to be a constant.

The equations for heat transport can be formulated in an equivalent way if we write them in terms of local heat content, $\tilde{q} = \rho C_p T$, where ρ, C_p, and T are the density, specific heat capacity, and temperature, respectively. With this, heat transport in the bulk of phase i is given by

$$\frac{\partial \tilde{q}_i}{\partial t} + \nabla \cdot (\vec{u}\tilde{q}_i) = \nabla \cdot \left(\frac{k_i}{\rho_i C_{p,i}} \nabla \tilde{q}_i \right), \tag{2.4}$$

where k is the heat conductivity. Heat balance at the interface gives

$$\frac{k_1}{\rho_1 C_{p,1}} \nabla_n \tilde{q}_1 = \frac{k_2}{\rho_2 C_{p,2}} \nabla_n \tilde{q}_2, \tag{2.5}$$

and thermal equilibrium can be written as

$$\frac{\tilde{q}_1}{\tilde{q}_2} = \frac{\rho_1 C_{p,1}}{\rho_2 C_{p,2}}. \tag{2.6}$$

The one-to-one correspondence between Eqs. (2.1)-(2.3) for mass and Eqs. (2.4)-(2.6) for heat is clear. As such, we utilize these forms of the equations to derive a generalized model that can apply to both mass and heat. We use the term scalar to refer to species concentration and heat content. It is worth remarking that the aforementioned formulation is based on the conserved variable. An equally valid approach would be to solve for the variable that is continuous across the interface, i.e., chemical potential for mass and temperature for heat. However, this approach is not preferred since it loses the discrete conservation property inherent in the former approach.

In this work, we neglect change in volume due to mass transfer. This is justified when the solute is in the dilute limit. Additionally, phase change is not considered; thus, the scalar evolution is one-way coupled to the phase field and momentum transport equations. We concern ourselves with incompressible flows and phase field models that result in hyperbolic tangent interfacial profiles at equilibrium. These models include traditional phase field models that are based on the Cahn-Hilliard or the Allen-Cahn equations (Anderson *et al.* 1998; Ding *et al.* 2007), in addition to the second-order conservative phase field model that was developed recently (Chiu & Lin 2011; Mirjalili *et al.* 2020),

$$\frac{\partial \phi}{\partial t} + \nabla \cdot (\vec{u}\phi) = \nabla \cdot \left[\gamma \left(\epsilon \nabla \phi - \phi \left(1 - \phi\right) \frac{\nabla \phi}{|\nabla \phi|} \right) \right], \tag{2.7}$$

where $\vec{n} = \nabla\phi/|\nabla\phi|$ is the normal vector and ϵ is the parameter that controls the diffuse interface thickness. In Eq. 2.7, ϕ is the phase field variable which is a smoothly varying function that can be interpreted as volume fraction of phase 1—fluid of pure phase 1 has $\phi = 1$, while fluid of pure phase 2 has $\phi = 0$. Note that the models derived in this work can also be applied to diffuse interface methods in compressible flows which attain hyperbolic tangent equilibrium profiles (see for instance Jain *et al.* (2020) and references therein).

2.2. *Model requirements*

Equations 2.1–2.6 can be readily applied to sharp interface methods. However, the concepts of bulk fluids and interfaces are not as well defined in phase field methods. Since in phase field models any point in space and time is a mixture of two immiscible phases, the governing equations introduced above do not directly apply. Rather, a model must be derived. In this work, we seek a model that satisfies the following requirements:

- Conservation: scalar must be locally and globally conserved in a discrete sense.
- Generalizability: must apply to all phase field methods with hyperbolic tangent equilibrium profiles and be usable for both heat and mass transfer.
- Consistency: the model should
  (a) reduce to the model presented in Jain & Mani (2020) when scalar diffusivity is zero in one of the phases.
  (b) asymptote to bulk equations given in Eqs. (2.1) and (2.4) away from the interfaces (ϕ tending to 0 or 1).
  (c) be equivalent to a single phase flow when the two phases have equal diffusivities (and other relevant properties).
  (d) predict long-time equilibrium profiles correctly (e.g., linear/flat in 1D)
  (e) not leak for the practical limit of large diffusivity ratios (e.g., $\mathcal{O}(10^4)$ for carbon dioxide transport in a water-air system).
- Convergence: as the mesh is refined and the interfacial region is made thinner, the model should converge to the true sharp interface solution.
- Positivity: physical constraints such as positivity of chemical species concentration must hold discretely.

To obtain a set of equations that result in a consistent and robust model for phase field methods, we assume an interfacial microstructure compatible with a diffuse interface and apply the above equations to control volumes containing sharp interfaces in the microstructure to derive the upscaled equations.

2.3. *Microscopic model*

In diffuse interface methods, a capillary interface of $\mathcal{O}(1$ nm) thickness is artificially made thick, on the order of the grid size, for numerical purposes. As explained above, because the system of equations is defined as a boundary value problem with clearly defined sharp interfaces that act as boundaries which are lacking in a diffuse interface method, direct application of Eqs. (2.1)-(2.6) is not possible. In order to eliminate the ambiguity in the governing equations for a diffuse interface between two immiscible phases, one can assume that the diffuse interface region has a microstructure consisting of well-defined sharp interfaces. In particular, in this work, we assume a microscopic model that is amenable to pen and paper analysis, shown schematically in Figure 1. This figure displays a one-dimensional diffuse interface with various levels of zoom-in. Figure 1(a) shows the smooth transition from one phase to the other. By zooming in onto the thin box with width $\mathcal{O}(\epsilon)$ within the transition zone of this figure, we can see the assumed microstructure. This microstructure, shown schematically in Figure 1(b), consists of fingers of one pure phase extending into the other. It is worth emphasizing that the interfaces shown in Figure 1(b) are sharp interfaces that separate pure phases from one another. As such, Eqs. 2.1-2.6 can be applied at this level. In accordance with the phase field models of interest, the fingers are assumed to have hyperbolic tangent profiles. We also intentionally assume that the thickness of the fingers is very small compared to the thickness of the diffuse interface (transition zone). In other words, Figure 1(b) is highly stretched in the

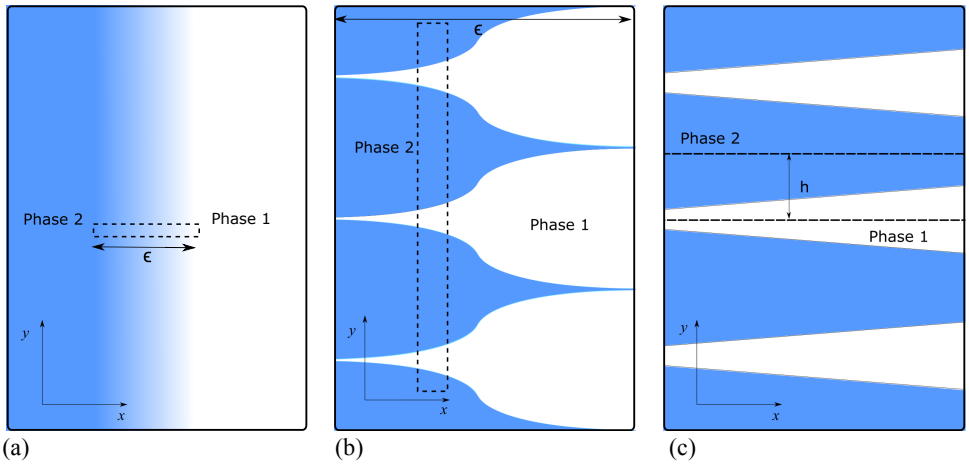

FIGURE 1. Schematic depiction of (a) a 1D diffuse interface, (b) the microstructure when one zooms in on a narrow window on the diffuse interface and (c) a close-up view of the microstructure, schematically showing that the fingers are assumed to be thin structures.

y direction. Zooming in on the box shown in Figure 1(b), a more accurate picture of the local microstructure can be obtained, shown schematically in Figure 1(c). This figure is demonstrating that the microstructure consists of long and thin structures with thickness h, where $h \ll \epsilon$.

2.4. *Model derivation*

Two-scalar models are necessary for capturing species concentration or heat content when the interface is not at thermodynamic equilibrium and/or the diffusivity (resistance) ratio is large. In this section, we derive a two-scalar model using a one-dimensional interface. Similar to the model of Jain & Mani (2020), the model solves for the amount of scalar in phase i per total volume, denoted $c_i(x)$ for $i = 1, 2$. The total amount of scalar per total volume, $c_1(x) + c_2(x)$, is conserved. Since the diffuse interface is not in thermodynamic equilibrium, the local concentration values are functions of both x and y in Figure 1, given by $\tilde{c}_i(x, y)$ for $i = 1, 2$. The y-averaged mean concentration values within each finger are then denoted $\bar{\tilde{c}}_1(x) = c_1(x)/\phi(x)$ and $\bar{\tilde{c}}_2(x) = c_2(x)/(1 - \phi(x))$.

It is useful to illustrate that the model of Jain & Mani (2020) for a confined scalar (no interfacial transfer) not only is compatible with the proposed microstructure, but also can be derived from this approach. To show this, imagine that a scalar is confined to phase 1 in Figure 1, then the equation governing the amount of scalar per total volume, $c_1(x)$, is given by

$$\frac{\partial c_1}{\partial t} + \frac{\partial}{\partial x}(\vec{u}c_1) = \frac{\partial}{\partial x}\left(D_1\phi\frac{\partial \bar{\tilde{c}}_1}{\partial x}\right) = \frac{\partial}{\partial x}\left[D_1\left(\frac{\partial c_1}{\partial x} - \frac{1-\phi}{\epsilon}\vec{n}c_1\right)\right]. \tag{2.8}$$

While the left-hand-side (LHS) terms represent the temporal and convective terms, the diffusive flux on the right-hand side (RHS) of the first equality can be explained by considering the microstructure. Since there is no interfacial transfer across the sharp interfaces, the local concentration is only a function of x and the local diffusive flux is

given by $D_1(\partial\bar{\tilde{c}}_1/\partial x)$. This flux has to then be weighted by the volume fraction of phase 1, $\phi(x)$, explaining the first equality in Eq. (2.8). Due to the hyperbolic tangent profile of the diffuse interface, the relation

$$\nabla\phi = \frac{\phi(1-\phi)}{\epsilon}\vec{n} \tag{2.9}$$

holds, which results in the second equality in (2.8), where the RHS is in terms of resolved variables. A similar PDE can be derived for $c_2(x)$. Here, we aim to derive the interfacial transfer terms that augment these PDEs to extend the work of Jain & Mani (2020) to arbitrary diffusivity ratios, D_1/D_2, and arbitrary jumps in scalar concentrations across the interface, denoted K_{eq}. For heat transfer, $K_{eq} = (\rho_1 C_{p,1})/(\rho_2 C_{p,2})$, while $K_{eq} = H$, for mass transfer. We seek $J(x)$ for

$$\frac{\partial c_1}{\partial t} + \frac{\partial}{\partial x}(\vec{u}c_1) = \frac{\partial}{\partial x}\left[D_1\left(\frac{\partial c_1}{\partial x} - \frac{1-\phi}{\epsilon}\vec{n}c_1\right)\right] + J(x), \tag{2.10}$$

$$\frac{\partial c_2}{\partial t} + \frac{\partial}{\partial x}(\vec{u}c_2) = \frac{\partial}{\partial x}\left[D_2\left(\frac{\partial c_2}{\partial x} + \frac{\phi}{\epsilon}\vec{n}c_2\right)\right] - J(x). \tag{2.11}$$

The local concentration can be decomposed into a mean component and a perturbation,

$$\tilde{c_i}(x,y) = \bar{\tilde{c}}_i(x) + \tilde{c_i}'(x,y). \tag{2.12}$$

Because of the assumed thin structure of the fingers in the microstructure, $h \ll \epsilon$, there is a quasi-steady balance between diffusion in x and y, yielding

$$\frac{\partial^2 \tilde{c_i}'}{\partial y^2} = -\frac{\partial^2 \bar{\tilde{c}}_i}{\partial x^2}, \tag{2.13}$$

for $i = 1, 2$. The thin structures are repeated periodically in the y direction with a period of $2h$. Let us focus on a half-period with thickness h, as shown in Figure 1(c). Consider a coordinate system on the lower dashed line, then symmetry boundary conditions hold for phase 1 at $y = 0$ and for phase 2 at $y = h$. Additionally, the perturbations have zero mean, i.e.,

$$\int_0^{\phi h} \tilde{c_1}'(x,y)dy = \int_{\phi h}^{h} \tilde{c_2}'(x,y)dy = 0. \tag{2.14}$$

Integrating Eq. (2.13) twice in y and using the symmetry boundary conditions in addition to Eq. (2.14), we can determine the perturbations in terms of the mean concentrations to be given by

$$\tilde{c_1}'(x,y) = -\frac{1}{2}\left(\frac{\partial^2 \bar{\tilde{c}}_1}{\partial x^2}\right)\left[y^2 - \frac{(\phi h)^2}{3}\right], \tag{2.15}$$

$$\tilde{c_2}'(x,y) = -\frac{1}{2}\left(\frac{\partial^2 \bar{\tilde{c}}_2}{\partial x^2}\right)\left\{(h-y)^2 - \frac{[(1-\phi)h]^2}{3}\right\}. \tag{2.16}$$

Two other conditions must be satisfied at the sharp interface located at $y = \phi h$. First, thermodynamic equilibrium must be enforced, $\tilde{c}_1(x, y = \phi h) = K_{eq}\tilde{c}_2(x, y = \phi h)$, which from Eqs. (2.15) and (2.16) results in

$$\phi^2\left(\frac{\partial^2 \bar{\tilde{c}}_1}{\partial x^2}\right) - K_{eq}(1-\phi)^2\left(\frac{\partial^2 \bar{\tilde{c}}_2}{\partial x^2}\right) = \frac{3}{h^2}(\bar{\tilde{c}}_1 - K_{eq}\bar{\tilde{c}}_2). \tag{2.17}$$

Second, after plugging in Eqs. (2.15) and (2.16) to find the diffusive fluxes in the y

direction, continuity of diffusive fluxes normal to the interface is written as

$$D_1\phi\left(\frac{\partial^2\bar{\tilde{c}}_1}{\partial x^2}\right)+D_2(1-\phi)\left(\frac{\partial^2\bar{\tilde{c}}_2}{\partial x^2}\right)=-D_1\frac{\partial\bar{\tilde{c}}_1}{\partial x}\frac{\partial\phi}{\partial x}+D_2\frac{\partial\bar{\tilde{c}}_2}{\partial x}\frac{\partial\phi}{\partial x}. \tag{2.18}$$

The interfacial transfer terms in Eqs. (2.10) and (2.11) are given by

$$J(x)=\frac{1}{h}D_1\left(\frac{\partial\tilde{c}_1{}'}{\partial y}\right)_{y=\phi h}-D_1\frac{\partial\bar{\tilde{c}}_1}{\partial x}\frac{\partial\phi}{\partial x}. \tag{2.19}$$

The first term on the RHS of Eq. (2.19) can be written in terms of $\partial^2\bar{\tilde{c}}_1/\partial x^2$ using Eq. (2.15). Invoking the sharp interface boundary conditions given by Eqs. (2.17) and (2.18), we can then find $\partial^2\bar{\tilde{c}}_1/\partial x^2$ and $\partial^2\bar{\tilde{c}}_2/\partial x^2$ in terms of lower-order derivatives. This results in

$$\begin{aligned}J(x)=\frac{1}{h^2}\frac{3D_1D_2}{K_{eq}D_1(1-\phi)+D_2\phi}(K_{eq}\bar{\tilde{c}}_2-\bar{\tilde{c}}_1)\\ -K_{eq}D_1(1-\phi)\frac{\partial\phi}{\partial x}\frac{-D_1\frac{\partial\bar{\tilde{c}}_1}{\partial x}+D_2\frac{\partial\bar{\tilde{c}}_2}{\partial x}}{K_{eq}D_1(1-\phi)+D_2\phi}-D_1\frac{\partial\bar{\tilde{c}}_1}{\partial x}\frac{\partial\phi}{\partial x}.\end{aligned} \tag{2.20}$$

The first term on the RHS of Eq. (2.20) originates from the diffusive flux in the y direction and has a very large $\mathcal{O}(1/h^2)$ prefactor. This term is indeed responsible for equilibrating the interface toward $\bar{\tilde{c}}_1(x)=K_{eq}\bar{\tilde{c}}_2(x)$. The timescale for this equilibrium is proportional to h^2. Since h is an artificial free parameter in the assumed microscopic model that is chosen to be very small, we have freedom in the exact form of the first term in Eq. (2.20). The other terms on the RHS of this equation, however, are responsible for the correct prediction of long-time equilibrium solutions. As such, if we utilize $\bar{\tilde{c}}_1(x)=K_{eq}\bar{\tilde{c}}_2(x)$ and the definitions of the mean concentration values, we can make the substitutions $\bar{\tilde{c}}_1=c_1+K_{eq}c_2$ and $\bar{\tilde{c}}_2=c_1/K_{eq}+c_2$ for these terms. With these choices, the final form of the transfer terms in one dimension is

$$J(x)=AD_m[K_{eq}c_2\phi-c_1(1-\phi)]-D_m\frac{\partial\phi}{\partial x}\frac{\partial(c_1+K_{eq}c_2)}{\partial x}, \tag{2.21}$$

where D_m is the mixed diffusivity, given by

$$D_m=\frac{D_1D_2}{K_{eq}D_1(1-\phi)+D_2\phi}. \tag{2.22}$$

Note that a new free parameter, A, is introduced in Eq. (2.21) in lieu of the prefactors in the first term on the RHS of Eq. (2.20). This free parameter is typically chosen to be a large constant. Moreover, the first term on the RHS of Eq. (2.20) has been multiplied by $\phi(1-\phi)$, a kernel that is active in the interfacial region. With these decisions, the final form of $J(x)$ in Eq. (2.21) is in terms of the resolved variables. The model is derived for a one-dimensional interface. The general model is then

$$\begin{aligned}\frac{\partial c_1}{\partial t}+\nabla\cdot(\vec{u}c_1)=\nabla\cdot\left[D_1\left(\nabla c_1-\frac{1-\phi}{\epsilon}\vec{n}c_1\right)\right]\\ +AD_m[K_{eq}c_2\phi-c_1(1-\phi)]-D_m\nabla\phi\cdot\nabla(c_1+K_{eq}c_2),\end{aligned} \tag{2.23}$$

$$\begin{aligned}\frac{\partial c_2}{\partial t}+\nabla\cdot(\vec{u}c_2)=\nabla\cdot\left[D_2\left(\nabla c_2+\frac{\phi}{\epsilon}\vec{n}c_2\right)\right]\\ +AD_m[c_1(1-\phi)-K_{eq}c_2\phi]+D_m\nabla\phi\cdot\nabla(c_1+K_{eq}c_2).\end{aligned} \tag{2.24}$$

Inspecting Eqs. 2.23 and 2.24 reveals the satisfaction of some of the important model requirements enlisted in Section 2.2. Firstly, by summing the two equations, it becomes clear that the transfer terms cancel out resulting in a conservative transport equation for $c_1 + c_2$, and therefore, $c_1 + c_2$ is a conserved scalar. We have already explained generalizability of the model in terms of application to various diffuse interface methods and the capability of predicting both heat and mass transport. In terms of consistency, item (a) is satisfied because $D_m = 0$ if one of the diffusivities is zero (see Eq. 2.22), resulting in zero interfacial transfer and reduction of the model to Eq. 2.8. Item (b) of the consistency requirements can also be observed from either of Eqs. 2.23 and 2.24. Let us consider Eq. 2.23 and the bulk of phase 1, i.e., ϕ tending to 1. In this region of the domain, $1 - \phi$, c_2 and $\nabla\phi$ all tend to zero, resulting in vanishing interfacial transfer, in addition to the diffusive flux reducing to $\nabla \cdot (D_1 \nabla c_1)$, which matches the bulk equations presented in Section 2.1. In Section 3 we will utilize canonical numerical tests with the main aim of demonstrating that the derived two-scalar model satisfies the remaining consistency requirements enlisted in Section 2.2. The presentation of numerical simulation results that confirm convergence and positivity of the two-scalar model are deferred to a forthcoming publication on this topic.

2.5. *One-scalar model*

Using the assumed microstructure and by assuming thermodynamic equilibrium at the interface, i.e., $\bar{\bar{c}}_1(x) = K_{eq}\bar{\bar{c}}_2(x)$, we can also derive a consistent one-scalar model for total species concentration/heat content per total volume. The interfacial transfer between the two-phases need not be considered in the derivation of this model. By considering the contribution of each phase to the diffusive fluxes and writing $\bar{\bar{c}}_1$ and $\bar{\bar{c}}_2$ in terms of c, ϕ and K_{eq}, the derived one-scalar model is given by

$$\frac{\partial c}{\partial t} + \nabla \cdot (\vec{u}c) = \nabla \cdot \left[D_{eff} \nabla \left(\frac{c}{K_{eff}} \right) \right], \tag{2.25}$$

where

$$D_{eff} = D_1 K_{eq} \phi + D_2 (1 - \phi), \tag{2.26}$$

and

$$K_{eff} = K_{eq} \phi + (1 - \phi). \tag{2.27}$$

This model is introduced here as an alternative approach for modeling scalar transport, against which we compare the two-scalar model.

2.6. *Computational approach*

Numerically, we use a Runge-Kutta (RK) explicit scheme to time-integrate Eqs. (2.23) and (2.24) coupled to Eq. (2.7). If solving for the flow field, we also couple these equations to the consistent momentum transport equations introduced in Mirjalili & Mani (2020). We use a standard staggered Cartesian grid where velocity vectors and all fluxes, including the scalar fluxes, are stored on their respective faces, while pressure, density, viscosity, scalar concentrations and the phase field variable are stored on cell centers. If solving for momentum, we compute density and viscosity linearly with respect to the phase field variable, while surface tension forces are computed via the continuum surface force method.

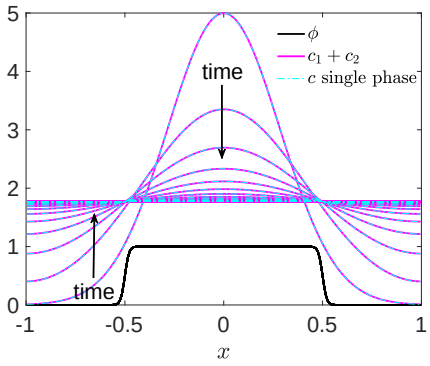

FIGURE 2. Evolution of $c_1 + c_2$ from the two-scalar, two-phase model plotted on top of the solutions from a single-phase calculation at the same time instants. The drop, for the two-phase calculation, is denoted using the phase field profile.

3. Numerical tests

In this section, we present numerical simulation results that confirm the satisfaction of all the consistency requirements enlisted in Section 2.2 by the two-scalar model. While we explained in Section 2.4 that some of the requirements can be checked by inspecting the model, here we numerically demonstrate that the consistency requirements (c)-(e) presented in Section 2.2 are met. All the simulations presented in this work are one-dimensional in nature and static. Multidimensional cases are deferred to a forthcoming journal article. For all the simulations, the domain is chosen to be $[-1, 1]$, the grid cell size is $\Delta x = 0.01$, and the parameters are taken to be $\epsilon = 0.01, \gamma = 1$, and $A = 1000$.

3.1. *Equivalence to single phase when $D_1 = D_2, K_{eq} = 1$*

If the diffusivities on the two sides of the interface are equal, then the presence of the interface has no effect on the transport of the scalar throughout the domain, thereby effectively reducing the problem setup to a pseudo-single-phase problem (consistency item (c) in Section 2.2). Here, we numerically verify this consistency for the two-scalar model. In particular, we set $D_1 = D_2 = K_{eq} = 1$ and use periodic boundary conditions to study the evolution of the system starting from $c_1(x, t = 0) = 5\exp(-4x^2), c_2(x, t = 0) = 0$, while the artificial drop has a diameter of 1 and is placed in the center of the domain. Figure 2 shows that the solution from the two-scalar, two-phase model matches very well with the numerical solution from a single-phase calculation with the same resolution and discretization.

3.2. *Flat equilibrium solutions*

A one-dimensional drop of phase 1 with diameter 1 is placed in the middle of the domain. The initial conditions are $c_1(x, t = 0) = 2\phi(x, t = 0)$ and $c_2(x, t = 0) = 0$ and we use periodic boundary conditions. The equilibrium solution is expected to be flat profiles within the drop and outside it with a jump based on the value of K_{eq}. In particular, $c_1 + K_{eq}c_2$ should be a flat profile at equilibrium.

In Figure 3(a), the evolution of c_1 and c_2 are plotted on top of the drop profile for a simulation performed using $D_1 = D_2 = K_{eq} = 1$. In Figure 3(b), at the same time instants, values of $c_1 + K_{eq}c_2 = c_1 + c_2$ are plotted, showing the correct flat profile at equilibrium.

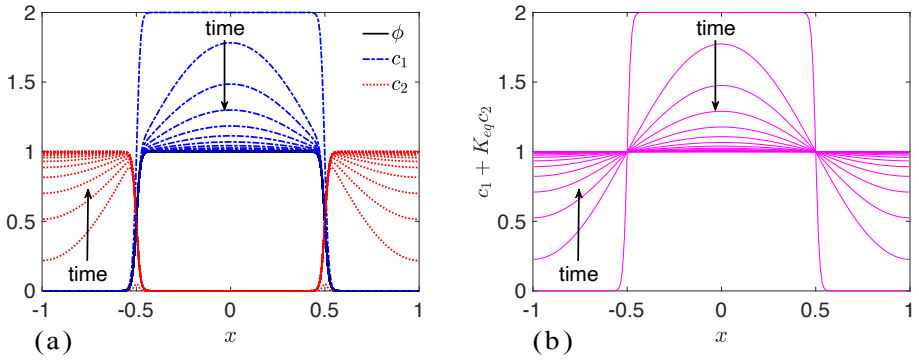

FIGURE 3. The evolution of (a) c_1 and c_2 plotted on top of the drop profile given by ϕ and (b) $c_1 + K_{eq}c_2$ plotted for simulations performed with $D_1 = D_2 = K_{eq} = 1$.

In Figure 4, for the same initial conditions and boundary conditions, simulation results for $K_{eq} = 1/3$ are illustrated. Figures 4(a,b) demonstrate how c_1, c_2 and $c_1 + K_{eq}c_2$ evolve in time for $D_1 = D_2 = 1$. Exploring the effect of the diffusivity ratio, Figures 4(c,d) demonstrate the evolution of c_1, c_2 and $c_1 + K_{eq}c_2$ for $D = 10, D_2 = 1$. Finally, Figures 4(d,e) serve the same purpose for $D_1 = 1, D_2 = 10$.

3.3. *Linear equilibrium solutions*

A one-dimensional drop of phase 1 with radius 1 is placed on the right half of the domain. The initial conditions are again $c_1(x, t = 0) = 2\phi(x, t = 0)$ and $c_2(x, t = 0) = 0$ and we use Dirichlet boundary conditions given by $c_1(x = -1, t) = c_2(x = -1, t) = 0$ and $c_1(x = 1, t) = 2, c_2(x = 1, t) = 0$. The equilibrium solutions are expected to be linear profiles within the drop and outside it, with slopes that are inversely proportionate to the diffusivity in each phase and a jump in accordance with the value of K_{eq}. In this case, $c_1 + K_{eq}c_2$ should consist of two lines with no jump across the interface at equilibrium.

In Figure 5(a), the evolution of c_1 and c_2 are plotted on top of the drop profile for a simulation performed using $D_1 = D_2 = K_{eq} = 1$. In Figure 5(b), $c_1 + K_{eq}c_2 = c_1 + c_2$ is plotted at the same time instants, showing the correct linear profile at equilibrium. We vary the diffusivity ratio, $D_1 = 10, D_2 = 1$, in the next simulation, shown in Figures 5(c,d). For this case the behavior of the solution is not monotonic with time in the phase with higher diffusivity. Finally, going back to $D_1 = D_2 = 1$, we test the effect of varying the interfacial jump, $K_{eq} = 1/3$, as depicted in Figures 5(e,f).

It must be emphasized that while the tests presented in this section might seem to have trivial solutions, the correct prediction of these solutions depends on the details of the two-scalar model presented in Eqs. (2.23) and (2.24). In particular, if the last transfer term in these equations were to be excluded, significant errors would arise in the solutions.

3.4. *Large diffusivity ratio*

As mentioned in Section 2.2, a very important limit for which we need the solutions from our models to be accurate is at large diffusivity ratios. Jain & Mani (2020) showed that the model presented in Eq. (2.8) prevents leakage for a confined scalar, whereas the naive one-scalar model presented in Section 2.5 results in significant leakage to the phase with zero diffusivity. As explained in Section 2.4, our two-scalar model [Eq. (2.23)] reduces to the confined scalar model in Eq. (2.8) when one of the diffusivities is zero, i.e., scalar

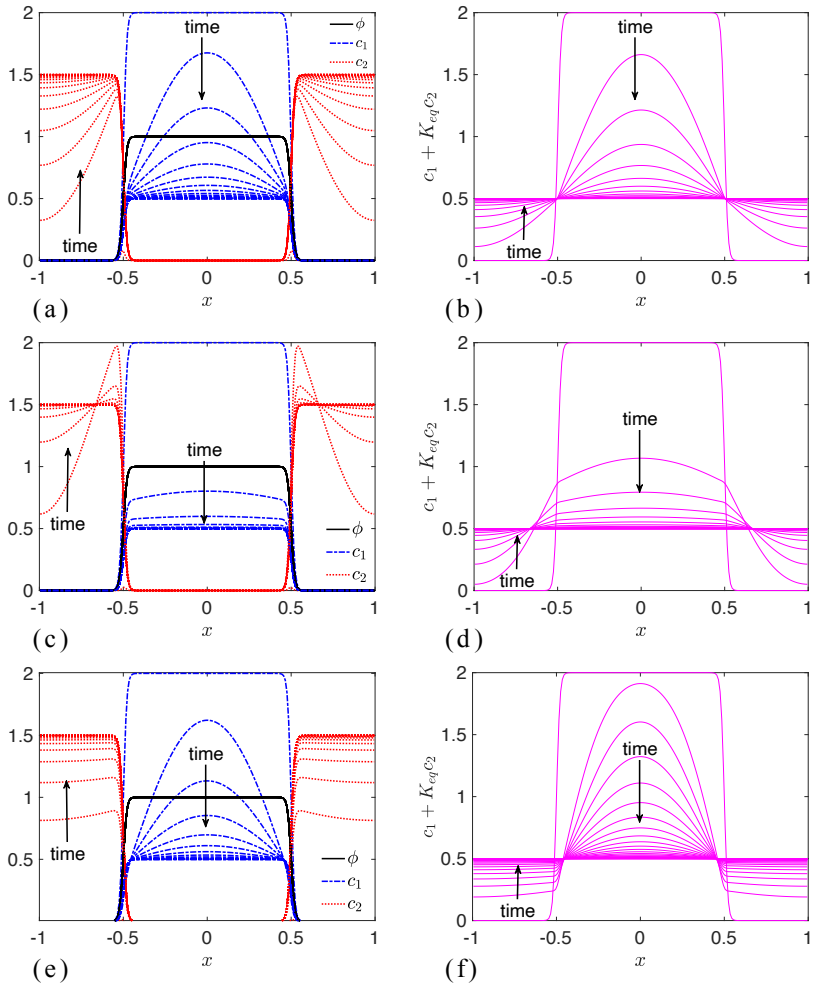

FIGURE 4. For jump conditions given by $K_{eq} = 1/3$, the evolution of (a) c_1 and c_2 plotted on top of the drop profile given by ϕ and (b) $c_1 + K_{eq}c_2$ plotted for simulations performed with $D_1 = D_2 = 1$, (c) c_1 and c_2 plotted on top of the drop profile given by ϕ and (d) $c_1+K_{eq}c_2$ plotted for simulations performed with $D_1 = 10, D_2 = 1$ and (e) c_1 and c_2 plotted on top of the drop profile given by ϕ and (f) $c_1 + K_{eq}c_2$ plotted for simulations performed with $D_1 = 1, D_2 = 10$.

is confined (consistency item (a) in Section 2.2). However, an important limit we study numerically here is large but finite diffusivity ratios to show that the derived two-scalar model satisfies consistency item (e) in Section 2.2. Figure 6 compares the performance of the two-scalar model against the one-scalar model for $D_1 = 1,\ D_2 = 10^{-4},\ K_{eq} = 1$. For the two-scalar model the initial conditions are $c_1(x, t = 0) = \phi,\ c_2(x, t = 0) = 0$, whereas for the one-scalar model the simulations are initialized with $c(x, t = 0) = \phi$. Figure 6(a) shows how well the two-scalar model can predict the evolution of the scalar as time progresses up to $t = 1$ compared with the results from the one-scalar model shown in Figure 6(b) for the same time instants that suffer from significant artificial leakage into phase 2.

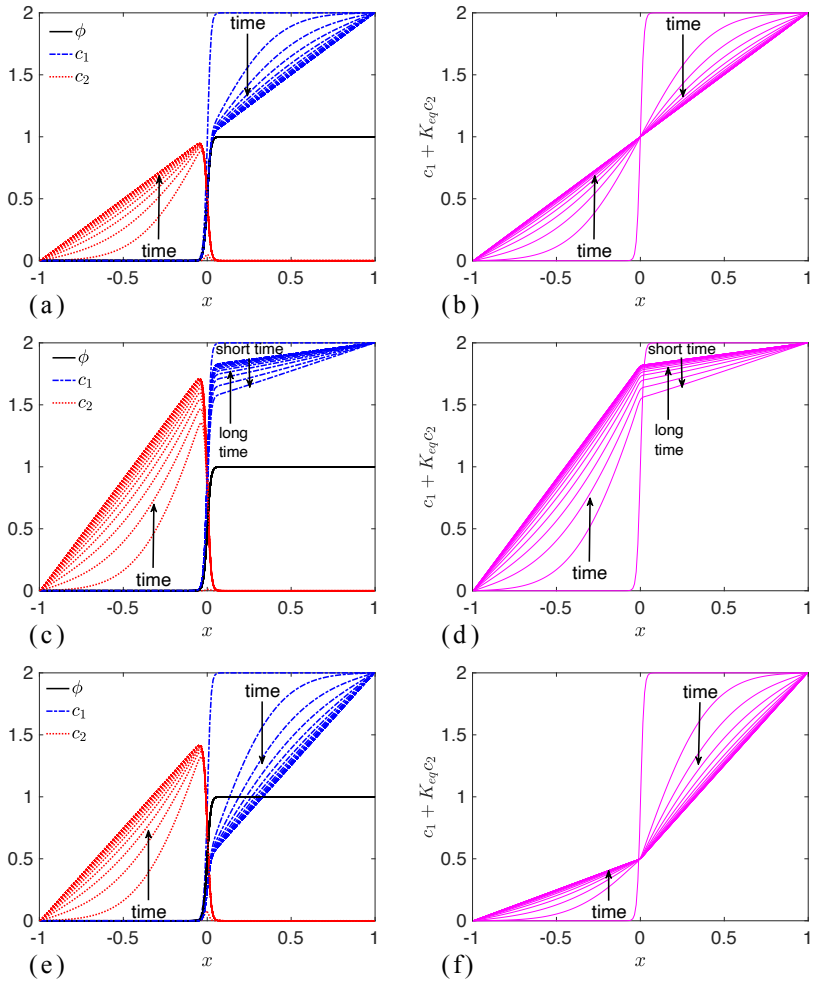

FIGURE 5. The evolution of (a) c_1 and c_2 plotted on top of the drop profile given by ϕ and (b) $c_1 + K_{eq}c_2$ plotted for simulations performed with $D_1 = D_2 = K_{eq} = 1$, (c) c_1 and c_2 plotted on top of the drop profile given by ϕ and (d) $c_1 + K_{eq}c_2$ plotted for simulations performed with $D_1 = 10, D_2 = K_{eq} = 1$ and (e) c_1 and c_2 plotted on top of the drop profile given by ϕ and (f) $c_1 + K_{eq}c_2$ plotted for simulations performed with $D_1 = D_2 = 1, K_{eq} = 1/3$.

4. Conclusions

In this study, we introduce a systematic approach for derivation of consistent PDE modifications for modeling multiphysics using phase field (diffuse interface) methods. Specifically, by assuming a microscopic model that is consistent with the interfacial profile and by applying the sharp interface equations within the microscopic structure, we analytically derive the upscaled equations for the evolution of conserved scalars within the framework of diffuse interface methods. The resulting model is a consistent heat/mass transfer model that can be applied to arbitrary diffusivity ratios and jump conditions. We validate the two-scalar model using canonical tests in 1D, showing in particular that it: converges to a single-phase calculation when the two phases are identical, predicts equi-

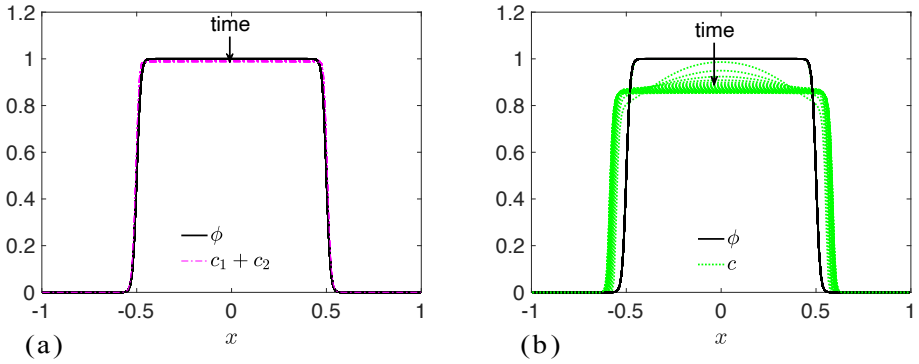

FIGURE 6. Evolution of the scalar field up to $t = 1$ plotted for $D_1 = 1,\ D_2 = 10^{-4},\ K_{eq} = 1$ using (a) the two-scalar model given in Eqs. (2.23),(2.24) and (b) the one-scalar model given in Eq. (2.25).

librium profiles accurately, and prevents leakage in the practical limit of large diffusivity ratios.

Acknowledgments

This material is based upon work supported by the Defense Advanced Research Projects Agency (DARPA) under agreement No. HR00112090065. S. S. Jain is supported by a Franklin P. and Caroline M. Johnson Fellowship from Stanford University. The authors thank Changxiao Shao for helpful comments on an early draft of this manuscript.

REFERENCES

ALKE, A., BOTHE, D., KROEGER, M. & WARNECKE, H. 2009 VOF-based simulation of conjugate mass transfer from freely moving fluid particles. *WIT Trans. Eng. Sci.* **63**, 157–168.

ANDERSON, D., MCFADDEN, G. & WHEELER, A. 1998 Diffuse-interface methods in fluid mechanics. *A*nnu. Rev. Fluid Mech. **30**, 139–165.

BALCÁZAR-ARCINIEGA, N., ANTEPARA, O., RIGOLA, J. & OLIVA, A. 2019 A level-set model for mass transfer in bubbly flows. *Int. J. Heat Mass Tran.* **138**, 335–356.

BERRY, J., DAVIDSON, M. & HARVIE, D. J. 2013 A multiphase electrokinetic flow model for electrolytes with liquid/liquid interfaces. *J. Comput. Phys.* **251**, 209–222.

BOTHE, D. & FLECKENSTEIN, S. 2013 A volume-of-fluid-based method for mass transfer processes at fluid particles. *Chem. Eng. Sci.* **101**, 283–302.

BOTHE, D., KOEBE, M., WIELAGE, K., PRÜSS, J. & WARNECKE, H.-J. 2004 Direct numerical simulation of mass transfer between rising gas bubbles and water. In Sommerfeld, E. (Ed.) *Bubbly Flows: Analysis, Modelling and Calculation.* Springer.

CHIU, P.H. & LIN, Y.T. 2011 A conservative phase field method for solving incompressible two-phase flows. *J. Comput. Phys.* **230**, 185–204.

DAVIDSON, M. R. & RUDMAN, M. 2002 Volume-of-fluid calculation of heat or mass transfer across deforming interfaces in two-fluid flow. *Numer. Heat Tr. B-Fund.* **41**, 291–308.

Deising, D., Bothe, D. & Marschall, H. 2018 Direct numerical simulation of mass transfer in bubbly flows. *Comput. Fluids* **172**, 524–537.

Ding, H., Spelt, P. D. & Shu, C. 2007 Diffuse interface model for incompressible two-phase flows with large density ratios. *J. Comput. Phys.* **226**, 2078–2095.

Fleckenstein, S. & Bothe, D. 2015 A volume-of-fluid-based numerical method for multi-component mass transfer with local volume changes. *J. Comput. Phys.* **301**, 35–58.

Jain, S. S. & Mani, A. 2020 Modeling transport of scalars in two-phase flows with a diffuse-interface method. arXiv:2011.10705vl [physics.flu-dyn].

Jain, S. S., Mani, A. & Moin, P. 2020 A conservative diffuse-interface method for compressible two-phase flows. *J. Comput. Phys.* p. 109606.

Kantarci, N., Borak, F. & Ulgen, K. O. 2005 Bubble column reactors. *Process Biochem.* **40**, pp. 2263–2283.

Kister, H. Z., Haas, J. R., Hart, D. R. & Gill, D. R. 1992 *Distillation design*, vol. 1. McGraw-Hill New York.

Lal, R. 2008 Carbon sequestration. *Philos. Trans. R. Soc. Lond. B Biol. Sci.* **363**, pp. 815–830.

Lefebvre, A. H. & McDonell, V. G. 2017 *Atomization and sprays*. CRC press.

Marschall, H., Hinterberger, K., Schüler, C., Habla, F. & Hinrichsen, O. 2012 Numerical simulation of species transfer across fluid interfaces in free-surface flows using OpenFOAM. *Chem. Eng. Sci.* **78**, 111–127.

Mehdi-Nejad, V., Mostaghimi, J. & Chandra, S. 2004 Modelling heat transfer in two-fluid interfacial flows. *Int. J. Numer. Meth. Eng.* **61**, 1028–1048.

Mirjalili, S., Ivey, C. B. & Mani, A. 2020 A conservative diffuse interface method for two-phase flows with provable boundedness properties. *J. Comput. Phys.* **401**, 109006.

Mirjalili, S., Jain, S. S. & Dodd, M. 2017 Interface-capturing methods for two-phase flows: an overview and recent developments. *Annual Research Briefs*, Center for Turbulence Research, Stanford University, pp. 117–135.

Mirjalili, S. & Mani, A. 2020 Consistent, energy-conserving momentum transport for simulations of two-phase flows using the phase field equations. *J. Comput. Phys.* p. 109918.

Nomura, T., Tsubota, M., Oya, T., Okinaka, N. & Akiyama, T. 2013 Heat storage in direct-contact heat exchanger with phase change material. *Appl. Therm. Eng.* **50**, pp. 26–34.

Orlebeke, D. & Orlebeke, J. K. 2009 Oxygenation of aqueous systems. US Patent App. 11/917,746.

Stephenson, T., Brindle, K., Judd, S. & Jefferson, B. 2000 *Membrane bioreactors for wastewater treatment*. IWA publishing.

Wang, J., Lu, P., Wang, Z., Yang, C. & Mao, Z.-S. 2008 Numerical simulation of unsteady mass transfer by the level set method. *Chem. Eng. Sci.* **63**, 3141–3151.

Williams, F. A. 2018 *Combustion theory*. CRC Press.

Yang, C. & Mao, Z.-S. 2005 Numerical simulation of interphase mass transfer with the level set approach. *Chem. Eng. Sci.* **60**, 2643–2660.

Zheng, X., Babaee, H., Dong, S., Chryssostomidis, C. & Karniadakis, G. 2015 A phase-field method for 3D simulation of two-phase heat transfer. *Int. J. Heat Mass Tran.* **82**, 282–298.